catalysts

MDPI

Article

CO_2 Hydrogenation to Synthetic Natural Gas over Ni, Fe and Co–Based CeO_2–Cr_2O_3

Chalempol Khajonvittayakul [1], Vut Tongnan [1], Suksun Amornraksa [1], Navadol Laosiripojana [2], Matthew Hartley [3] and Unalome Wetwatana Hartley [1,2,*]

[1] Chemical and Process Engineering, The Sirindhorn International Thai-German Graduate School of Engineering (TGGS), King Mongkut's University of Technology North Bangkok, Bangkok 10800, Thailand; chalempol.k-cpe2016@tggs.kmutnb.ac.th (C.K.); vut.t-dcpe2018@tggs.kmutnb.ac.th (V.T.); suksun.a@tggs.kmutnb.ac.th (S.A.)

[2] Joint Graduate School of Energy and Environment (JGSEE), King Mongkut's University of Technology Thonburi, Bangkok 10140, Thailand; navadol@jgsee.kmutt.ac.th

[3] Department of Chemical Engineering, Faculty of Engineering, King Mongkut's University of Technology North Bangkok, Bangkok 10800, Thailand; matthew.h@eng.kmutnb.ac.th

* Correspondence: unalome.w.cpe@tggs-bangkok.org; Tel.: +66-2555-2930

Abstract: CO_2 methanation was studied over monometallic catalyst, i.e., Ni, Fe and Co; on CeO_2-Cr_2O_3 support. The catalysts were prepared using one-pot hydrolysis of mixed metal nitrates and ammonium carbonate. Physicochemical properties of the pre- and post-exposure catalysts were characterized by X-Ray Powder Diffraction (XRD), Hydrogen Temperature Programmed Reduction (H_2-TPR), and Field Emission Scanning Electron Microscope (FE-SEM). The screening of three dopants over CeO_2-Cr_2O_3 for CO_2 methanation was conducted in a milli-packed bed reactor. Ni-based catalyst was proven to be the most effective catalyst among all. Thus, a group of NiO/CeO_2-Cr_2O_3 catalysts with Ni loading was investigated further. 40 % NiO/CeO_2-Cr_2O_3 exhibited the highest CO_2 conversion of 97.67% and CH_4 selectivity of 100% at 290 °C. The catalytic stability of NiO/CeO_2-Cr_2O_3 was tested towards the CO_2 methanation reaction over 50 h of time-on-stream experiment, showing a good stability in term of catalytic activity.

Keywords: synthetic natural gas; CO_2 methanation; Ni-based catalysts; CeO_2-Cr_2O_3 catalyst

check for updates

Citation: Khajonvittayakul, C.; Tongnan, V.; Amornraksa, S.; Laosiripojana, N.; Hartley, M.; Hartley, U.W. CO_2 Hydrogenation to Synthetic Natural Gas over Ni, Fe and Co–Based CeO_2–Cr_2O_3. *Catalysts* **2021**, *11*, 1159. https://doi.org/10.3390/catal11101159

Academic Editor: Wojciech Gac

Received: 29 August 2021
Accepted: 22 September 2021
Published: 26 September 2021

Publisher's Note: MDPI stays neutral with regard to jurisdictional claims in published maps and institutional affiliations.

Copyright: © 2021 by the authors. Licensee MDPI, Basel, Switzerland. This article is an open access article distributed under the terms and conditions of the Creative Commons Attribution (CC BY) license (https://creativecommons.org/licenses/by/4.0/).

1. Introduction

Global warming has caused several serious impacts on the environment in recent years. Increasing CO_2 emission is anthropogenic in origin and is the main cause of global warming. Nowadays, many studies focused on two strategies to reduce atmospheric CO_2 concentration; through carbon capture and CO_2 conversion to biofuels [1,2]. The captured CO_2 can be utilized and converted into fuels and chemicals via chemical processes such as dry reforming of methane for synthesis gas production, or CO_2 hydrogenation to CH_4, methanol or higher alcohols [3]. CO_2 methanation is one of the promising processes which involves carbon recycle from abundant CO_2. Methane, as a product of CO_2 hydrogenation, is considered versatile and flexible as it can be injected directly into existing natural gas pipelines, or utilized as a raw material for chemical production [4]. This CO_2 hydrogenation can be looked at as Power-to-Gas process (PtG) by its means to store (and transport) energy in the form of natural gas [5]. The process refers to a conversion of renewable electricity to a gaseous energy carrier via two pathways: (1) H_2 production by water electrolysis, where wind or solar energy technologies could be integrated; and (2) H_2 conversion to CH_4, by methanation reaction with external CO_2 capture [6]. CO_2 methanation was firstly discovered and proposed as the Sabatier reaction: $CO_2 + 4H_2 \leftrightarrows CH_4 + 2H_2O$, $\Delta H_r^{298} = -164.8$ kJ·mol^{-1} [7]. Although the reaction is highly exothermic and thermodynamically favored at high pressures/low temperatures (<400 °C) [4,8], there are significant kinetic

limitations due to the high stability of CO_2. Furthermore, heat accumulation from the reaction generally causes severe hotspots in the reactor, due to the heat transfer limitation within the process, leading to the catalyst deactivation and shortened catalyst lifespan [9]. Moreover, low operating temperature is favorable for CO disproportionation reaction ($2CO \leftrightarrow CO_2 + C$, $\Delta H_r^{298} = -172.4\ kJ \cdot mol^{-1}$), resulting in unwanted coke deposition. In order to obtain the highest possible methane yield, it is necessary to invent a catalyst which enhances the reaction's activity, withstands sintering and counters the coking phenomenon. Various active metals (such as Ni, Fe, Co, Ru, Rh, and Pd) have been used as an active site while metal oxides (such as CeO_2, La_2O_3, MgO, γ-Al_2O_3, SiO_2, TiO_2, and ZrO_2) have been useful as a support in a catalyst system for the CO_2 methanation reaction [3,10–13]. Amongst these materials, CeO_2 is so far found to be the most interesting support due to its high oxygen storage capacity (OSC) and its ability to disperse the active site [14]. In addition, CeO_2 could promote the interaction between support and metal active component, such that the growth and dispersion of the metal active particles can be well distributed and controlled throughout the surface of the support, leading to the higher CO_2 conversion [15]. The number oxygen vacancy can be tailor-made by substituting smaller transition metal ions (e.g., chromium ions) into CeO_2. The higher number of lattice oxygen can combust coke deposits and reduce the chance of sintering [13,16–18]. According to previous research, Ni-, Fe-, Co doped on CeO_2 have shown relatively high activities for CO_2 methanation and possessed high stability when tested for 15 to 50 h reaction times [19–23].

In this work, Ni-, Fe- and Co- based CeO_2/Cr_2O_3 were prepared using the one-pot hydrolysis method. The level of metal loading, operating temperature, reduction temperature and other relevant variables were observed as all of these parameters are well-known to influence the catalytic performance of the catalysts [24,25]. The physicochemical properties of the synthesized catalysts were examined, comparing pre- and post-exposure by X-Ray Diffractometer (XRD), Hydrogen Temperature-Programmed Reduction (H_2-TPR), and Field Emission Scanning Electron Microscopes (FE-SEM). The catalyzation of CO_2 methanation was conducted in a milli-packed bed reactor under atmospheric pressure where the operating temperature was varied from 200 to 350 °C. The reduction temperatures of 500 and 700 °C were chosen (via H_2-TPR) for comparison purposes. WSHV was fixed at 27,624 $mL \cdot h^{-1} \cdot g_{cat}{}^{-1}$, and the stoichiometric reactants ratio was kept at 4 for all the experiments.

2. Methodology

2.1. Catalyst Powder-Formed Preparation

Forty percent (by weight) x/CeO_2-Cr_2O_3 (where x = Ni, Fe, and Co) catalysts were synthesized by a single step preparation using $(NH_4)_2CO_3$ (PANREAC, 30% NH_3) as a hydrolysis agent, the details of which are outlined in [3]. The relevant nitrate precursors $Ni(NO_3)_2 \cdot 6H_2O$ (CARLO ERBA, Cornaredo, Italy, ≥99.0%), $Fe(NO_3)_3 \cdot 9H_2O$ (UNIVAR, Donners Grove, IL, UAS, ≥99.0%), $Co(NO_3)_2 \cdot 6H_2O$ (CARLO ERBA, ≥99.0%), $Ce(NO_3)_3 \cdot 6H_2O$ (ALDRICH, St. Louis, MO, USA, ≥99.0%), and $Cr(NO_3)_2 \cdot 6H_2O$ (ACROS, Merelbeke, Belgium, ≥99.0%) were dissolved in 50 mL distilled water where the ratio of active metal (Ni, Fe, and Co) to support (1 to 1 of CeO_2/Cr_2O_3) was fixed at 40 to 60 by weight. Two molar $(NH_4)_2CO_3$ solution was gradually dropped into the nitrate solutions until the pH reached 8.8–9.0. The mixture was continuously stirred while heated to 80 °C for 3 h. The solution's temperature was then raised again to 120 °C to evaporate water and a dark blue gel was slowly obtained. The resulting material was then calcined in moving air at 500 °C with 10 °C/min of heating for 24 h before the black powder of the catalyst was achieved. The catalyst powder was then pressed, crushed, and sieved to gain its uniform particle size ranging from 75 to 180 μm in order to avoid pressure drop that could occur across the catalyst bed.

2.2. Characterizations

XRD analysis (Malvern PANalytical diffractometer)was performed using CuKα radiation (with λ = 1.5418 Å, 40 kV, 15 mA). The diffractogram patterns were recorded

over 2-theta ranging from 10 to 80° with a scanning speed of 0.02° per second. The catalyst's phase structures were identified using JCPDS cards (Joint Committee on Powder Diffraction Standards).

The optimal reduction temperature of the catalyst was screened using an in situ H_2-TPR technique which was carried out in our lab-scale conventional packed-bed reactor, connected to a Quadrupole Mass Spectrometer (PFEIFFER, MS, Omnistar GSD 320, HAKUTO) operated in a SEM-MID mode. A total of 0.5 g of the catalyst sample was packed in a quartz tube reactor (i.d. = 10 mm) and pre-treated in 10% O_2/Ar at 500 °C for 1 h, followed by Ar purging to clean the catalyst's surface from any possible absorbed impurities. After the system reached ambient temperature, 5 % H_2/Ar was introduced through the catalyst's bed with a total flowrate of 100 mL·min^{-1} while the temperature was elevated to 950 °C at 5 °C/min.

Surface morphology and micro-structure of the catalysts, both pre- and post-exposure, were investigated using a Field Emission Scanning Electron Microscopes (FE-SEM, SU-8230 Hitachi, Japan) with an accelerating voltage of 15 kV.

2.3. CO_2 Methanation Activity in a Packed-Bed Reactor

CO_2 methanation was performed in a tubular packed-bed reactor under atmospheric pressure. A total of 0.2 g of catalyst was placed between two layers of quartz wool in the middle of the reactor (i.d. = 4 mm). The catalyst was reduced in 100 mL·min^{-1} of pure H_2 for 2 h at the achieved reduction temperature (from H_2-TPR where NiO reduced to metallic Ni at 500 °C while Co_2O_3 and Fe_3O_4 reduced to metallic Co and Fe at 850 °C) from the prior reaction. Next, the process was cooled down to the desired operating temperature, varying at 200, 210, 230, 250, 270, 290, 310, and 350 °C. Ar was purged in between to remove any excess H_2. The mixture of gaseous reactant, CO_2:H_2:Ar at a ratio of 1:4:5 by volume, was injected through the catalyst's bed. Total flow rate was set at 90 mL·min^{-1}, giving WSHV at 27,624 mL·h^{-1}·$g_{cat}{}^{-1}$. Moisture was condensed as a by-product using a cooler oil bath at the bottom of the reactor. After the process approached equilibrium, the dried gas products were automatically analyzed using gas chromatography coupled with a TCD detector (Shimadzu GC-2014ATF) every 7 min for 1 h. CO_2 conversion (X_{CO2}), CH_4 selectivity (S_{CH4}), and CH_4 yield (Y_{CH4}) were calculated using the following formulas:

$$CO_2\ conversion,\ X_{CO_2}\ [\%] = \left(\frac{F^{in}_{CO_2} - F^{out}_{CO_2}}{F^{in}_{CO_2}}\right) \times 100\% \quad (1)$$

$$CH_4\ selectivity,\ S_{CH_4}\ [\%] = \left(\frac{F_{CH_4}}{F_{CH_4} + F_{CO}}\right) \times 100\% \quad (2)$$

$$CH_4\ yield,\ Y_{CH_4}\ [\%] = \frac{X_{CO_2} \times S_{CH_4}}{100} \quad (3)$$

$F^{in}_{CO_2}$ and $F^{out}_{CO_2}$ represent volumetric flow rate of CO_2 in the feed stream and outlet stream, respectively, whereas F_{CH_4} and F_{CO} denote the volumetric flow rate of the product gas stream, CH_4 and CO, respectively.

3. Results and Discussion

3.1. Characterizations

3.1.1. XRD

XRD patterns of all the fresh catalysts (calcined in moving air at 500 °C) were achieved as shown in Figure 1. CeO_2-Cr_2O_3 (■), as major crystals, were found in all samples and appeared to possess fluorite cubic structure [26], having two-theta position peaks at 28.57, 33.12, 47.49, 56.38, 58.94, 69.42, 76.74, 79.33, 88.44, and 95.34°. All the dopants, NiO (●), Fe_2O_3 (♦), and Co_3O_4 (▲) appeared as minor crystalline phases as shown in Figure 1a–c, respectively. NiO peaks were found at 37.31, 43.35, 63.00, and 75.49° (JCPDS No. 01-073-1519); whereas Fe_2O_3 peaks appeared at 24.19, 33.28, 35.68, 40.99, 49.57, 54.32, 62.64, and

64.15 (JCPDS No. 01-076-4579); and Co_3O_4 peaks were detected at 33.06, 36.67, 44.59, 59.08, and 64.92 (JCPDS No. 01-078-5631). Pure phase Cr_2O_3 was found in Co_3O_4-CeO_2-Cr_2O_3 at 36.34, 44.60, 58.357, and 63.204° (JCPDS No. 00-001-1294), indicating that Cr_2O_3 cannot fully incorporate into the CeO_2 lattice. This inhomogeneous solid solution depends on the size of ionic radii of the solutes. The ionic radius of Ce^{3+} appeared the largest (1.101 Å), followed by Cr^{3+} (0.80 Å) and Co^{4+} (0.61 Å) [27,28]. Thus, the Co^{4+} ion was able to compete with Cr^{3+} in becoming embedded into the CeO_2 lattice, creating $CeCoO_3$ perovskite [27,29], as it can be seen in Figure 1c. This phenomenon could cause a decay in the catalyst's catalytic performance due to the loss of active sites, in this case, Co_3O_4. In addition, the average crystallite size of the NiO, Fe_2O_3, and Co_3O_4 on CeO_2-Cr_2O_3 were calculated using the Scherrer's equation at 14.56, 25.03, and 25.60 nm, respectively. The smaller active site could perhaps accommodate reactants better, rendering the chance of higher catalytic performance.

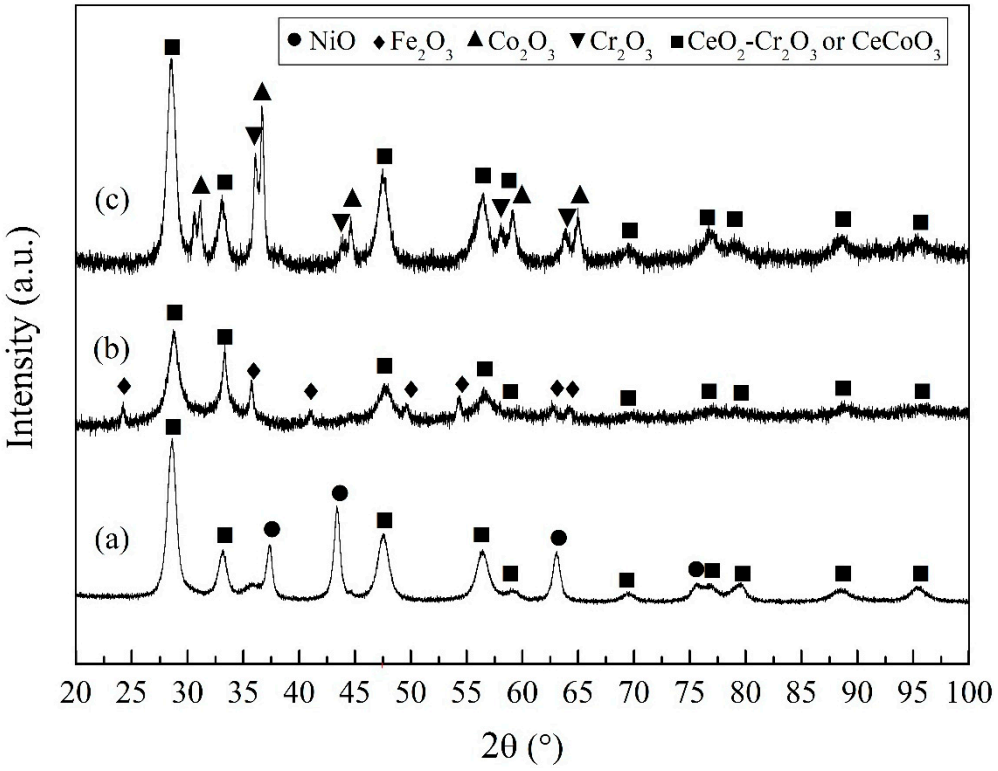

Figure 1. XRD patterns of (**a**) 40% NiO/CeO_2-Cr_2O_3, (**b**) 40% Fe_2O_3/CeO_2-Cr_2O_3, and (**c**) 40% Co_3O_4/CeO_2-Cr_2O_3 after calcined at 500 °C, where NiO (●), Fe_2O_3 (♦), Co_3O_4 (▲), Cr_2O_3 (▼), and CeO_2-Cr_2O_3 (■) phases.

3.1.2. H_2-TPR

Figure 2 shows the reduction profiles of pure CeO_2 (a), CeO_2-Cr_2O_3 (b), NiO/CeO_2-Cr_2O_3 (c), Fe_2O_3/CeO_2-Cr_2O_3 (d), and Co_3O_4/CeO_2-Cr_2O_3 (e) catalysts. Pure CeO_2 (a) had 2 small reduction peaks at 570 and >950 °C, corresponding to the surface reduction and bulk reduction of CeO_2, respectively [30]. The first reduction peak of CeO_2-Cr_2O_3 (b) appeared at 480 °C, where Cr^{6+} ions were reduced to Cr^{3+} ions. The reduction peak at 565 °C and >950 °C corresponded to the reduction of CeO_2-Cr_2O_3 at surface and bulk oxygen, respectively [30–33]. Substitution of Cr_2O_3 into CeO_2 was reported to enhance oxygen vacancy of the catalyst system [16,18,34], in which its H_2 consumption was proven to be significantly higher than the pure CeO_2.

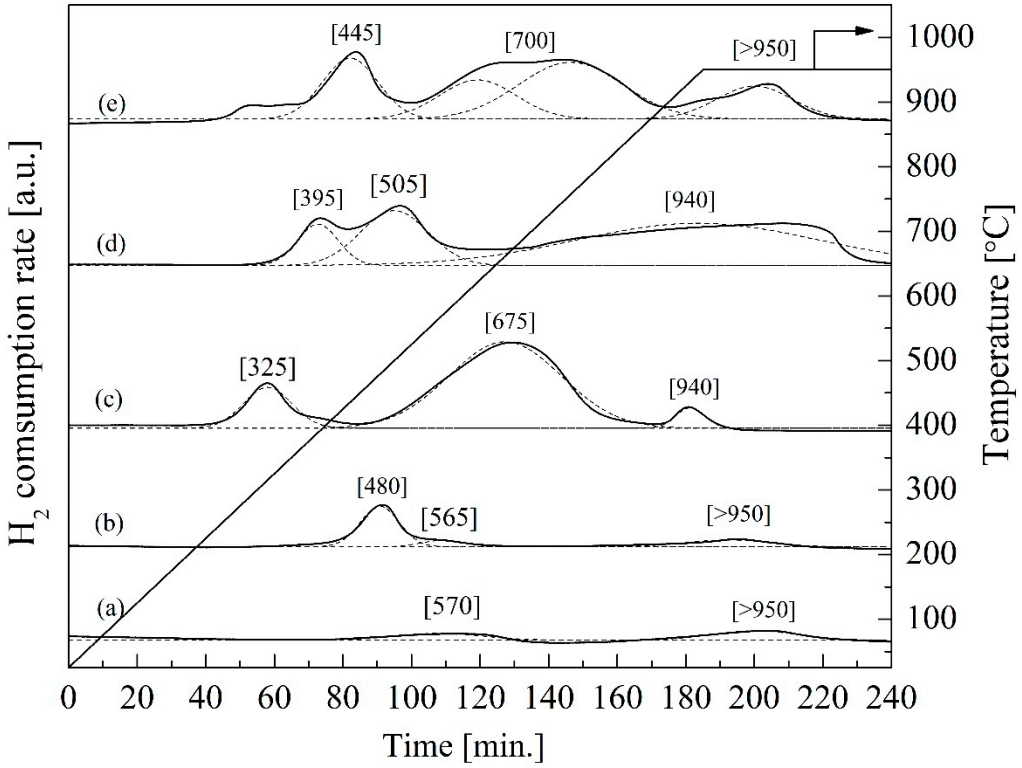

Figure 2. H_2-TPR profiles of (**a**) pure CeO_2, (**b**) CeO_2-Cr_2O_3, (**c**) 40%wt. NiO/CeO_2-Cr_2O_3, (**d**) 40%wt. Fe_2O_3/CeO_2-Cr_2O_3, and (**e**) 40%wt. Co_2O_3/CeO_2-Cr_2O_3 catalyst calcined at 500 °C.

Three distinct peaks at 325, 675, and 940 °C were found for NiO/CeO_2-Cr_2O_3 catalyst (c). The first two peaks were identical to the reduction of Ni^{3+} to Ni^{2+} and to the reduction of Ni^{2+} to metallic nickel, respectively [34–36]. Some reduction of Cr^{6+} ions to Cr^{3+} ions could be combined in the first peak, whereas the second and the third peaks represented the reduction of the Cr_2O_3 incorporated within the CeO_2 structure at the surface and bulk level, respectively. For Fe_2O_3/CeO_2-Cr_2O_3 (d), the first peak appeared at 395 °C, representing the reduction of Cr^{6+} ions to Cr^{3+} ions, whereas its second and third peaks at 505 and 940 °C were attributed to the reduction of CeO_2-Cr_2O_3 at the surface and bulk levels, respectively. The two reduction peaks observed at 505 °C and between 700 to 950 °C also represented the reduction of Fe_2O_3 to Fe_3O_4 and reduction of Fe_3O_4→FeO→metallic Fe, respectively [37,38]. Co_2O_3/CeO_2-Cr_2O_3 (e) was detected at 445, 700, and >950 °C, and associated with (1) the reduction of Cr^{6+} ions to Cr^{3+} ions, (2) the reduction of Co^{3+} ions to Co^{2+} ions and the reduction of CeO_2-Cr_2O_3 (and/or $CeCoO_3$ perovskite) with surface oxygen, and (3) the reduction of Co^{2+} ions to metallic Co, and the reduction of CeO_2-Cr_2O_3 (and/or $CeCoO_3$ perovskite) with bulk oxygen [39]. The catalyst's oxygen deficiency and number of active sites were interpreted from the hydrogen consumption, which was compared amongst all the catalysts and ordered as: NiO/CeO_2-Cr_2O_3 > Fe_2O_3/CeO_2-Cr_2O_3 > Co_2O_3/CeO_2-Cr_2O_3.

3.2. Catalytic Performance Test

3.2.1. Choice of the Monometallic

Catalytic performance, in terms of CO_2 conversion (Figure 3 (left)) and CH_4 selectivity (Figure 3 (right)), of all the prepared catalysts was determined at various operating temperatures, ranging from 200 to 350 °C. CO_2 conversion tended to increase with increasing temperature for all catalysts. Amongst all the selected metals, Ni was proven as the best monometallic active site for CeO_2-Cr_2O_3, considering CO_2 conversion, which was much higher than other metals (Fe and Co) starting at 260 °C. The highest CO_2 conversion over Ni/CeO_2-Cr_2O_3 was achieved at 290 °C, giving CO_2 conversion of 90.19%. However, CO_2

conversion decreased when the temperature was higher than 330 °C, due to its thermodynamic limitation [3,40,41]. In terms of CH_4 selectivity, Ni also showed the best performance by giving complete selectivity at 100% during all temperatures (from 200 to 360 °C), followed by Fe which offered 94% of CH_4 selectivity at its equilibrium at 290 °C. On the other hand, catalytic performance of Co as the monometallic dopant was incomparable to that of the other two, as it gave no reaction at low temperature (below 260 °C) and reached its maximum at 24% of CH_4 selectivity at 270 °C. The CH_4 selectivity was decreased at temperatures higher than 270 °C. This was due to the formation of CO as an unwanted product from the reverse water-gas shift reaction [19,42].

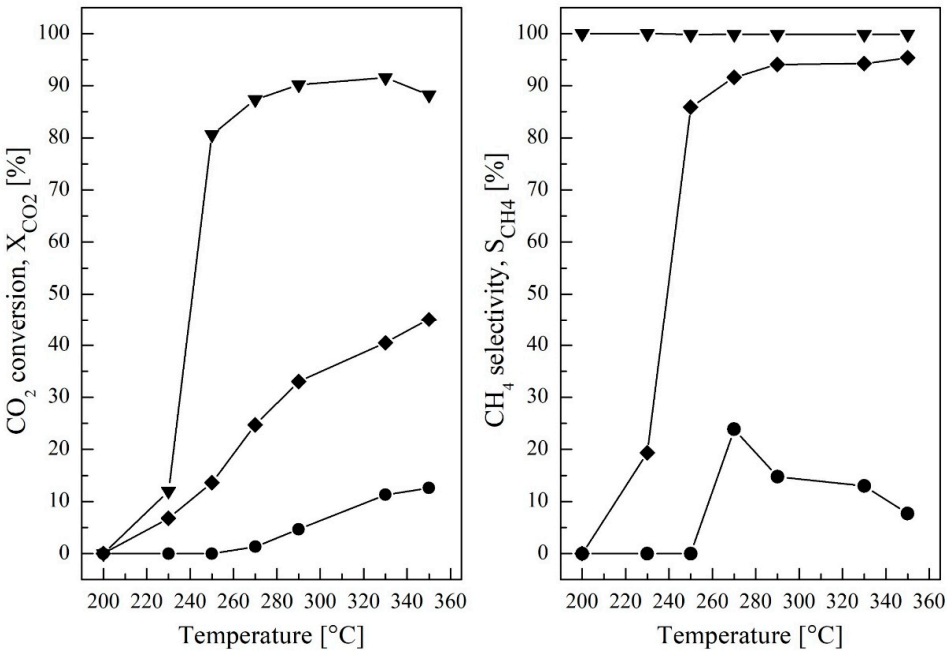

Figure 3. Catalytic performance of CO_2 methanation in terms of CO_2 conversion (**Left**) and CH_4 selectivity (**Right**) over different metals: (▼) Ni; (♦) Fe; and (●) Co; on CeO_2-Cr_2O_3 support.

3.2.2. Effect of Metal Content on Catalytic Performance

The influence of metal content, doped on CeO_2-Cr_2O_3, towards CO_2 methanation was investigated over Ni-/CeO_2-Cr_2O_3, where the Ni level was varied at 10, 20, 30, 40 and 50% by weight. Figure 4 showed that the percentage of all the selected Ni contents exhibited the same trend, where CO_2 conversion was increased with increasing temperature and increasing amount of Ni content. The nickel content represented the amount of the active site for CO_2 methanation reaction, thus, the higher level of Ni was unsurprisingly improved the efficiency of the reaction [41,43–45]. However, excess Ni loading could cause other problems, i.e., pore blockage, coagulation and obstruction of nano-channels [46–48]. For this reason, there was only a small difference in CO_2 conversion, between using 40% and 50% Ni loading.

3.2.3. Effect of Reduction Temperature on Catalytic Performance

Two different reduction temperatures, at 500 and 700 °C, were selected for this study. Figure 5 presents relationship between CO_2 conversion and reduction temperature of the catalyst at different operating temperatures. The results showed that the catalyst which reduced at 500 °C gave the highest CO_2 conversion for all of the temperature ranges, compared to the one reduced at 700 °C. In addition, the decrease in CO_2 conversion at the higher reduction temperature (700 °C) could also be the effect of the catalyst's sintering, resulting in a lower number of active sites [49].

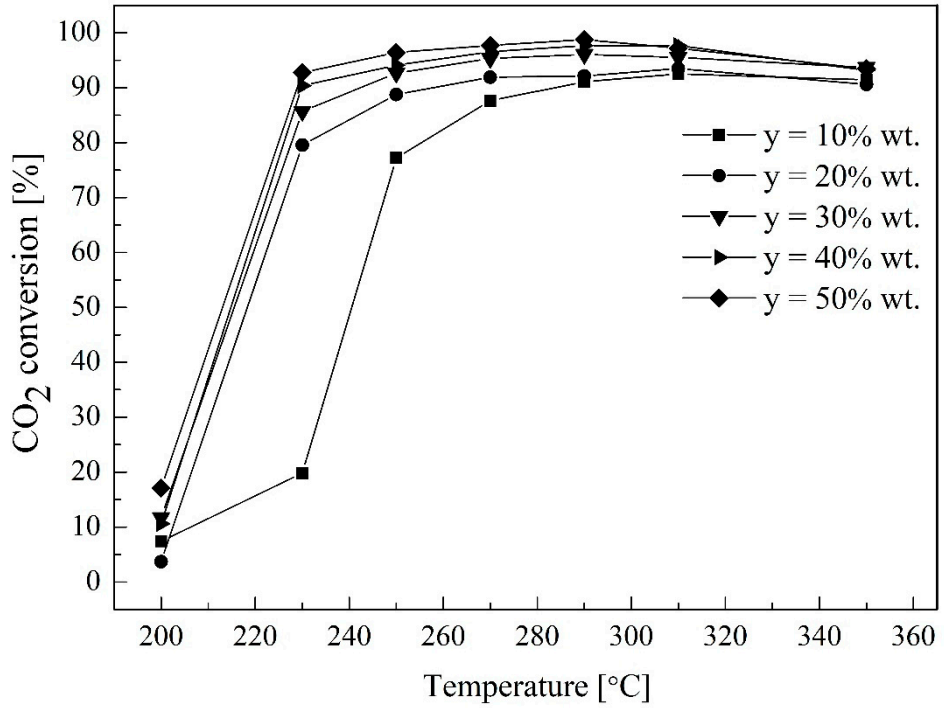

Figure 4. Catalytic performance of y %wt. NiO/CeO_2-Cr_2O_3 catalyst for CO_2 methanation.

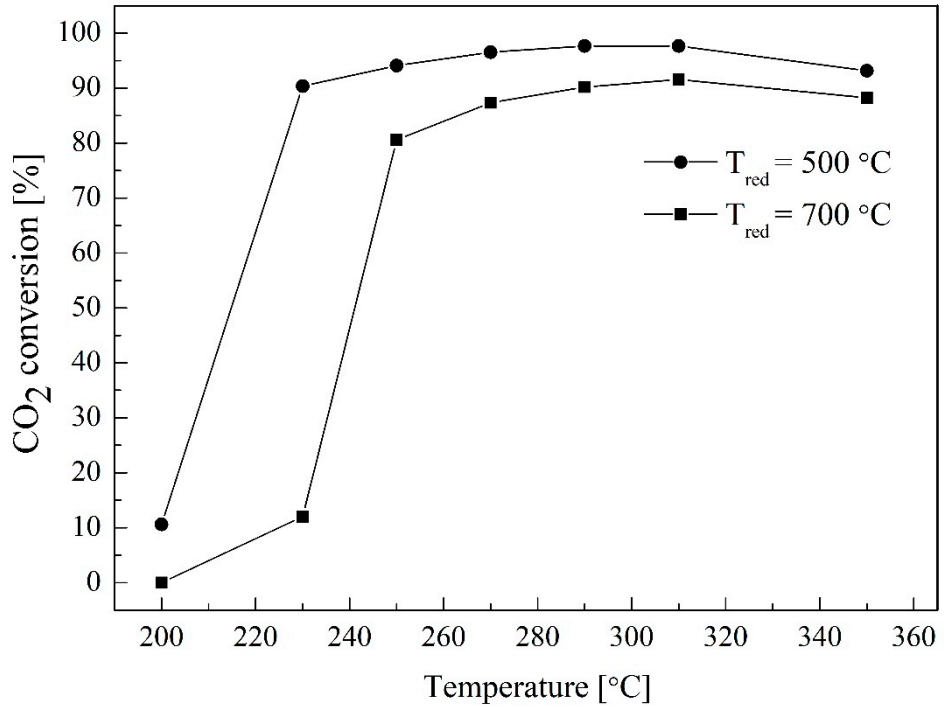

Figure 5. The catalytic performance with different reduction temperature using Ni-based on CeO_2-Cr_2O_3 catalyst.

3.3. Catalytic Stability

The catalytic stability of the NiO/CeO_2-Cr_2O_3 was measured in term of CO_2 conversion and CH_4 selectivity, illustrated in Figure 6. Approximately 97% of CO_2 conversion and 100% of CH_4 selectivity were achieved and maintained during 50 h of reaction time. XRD and SEM techniques were utilized for pre- and post-exposure characterization. XRD patterns of fresh NiO/CeO_2-Cr_2O_3 catalyst was compared with the post-exposure one

after the stability test, shown in Figure 7. Although both look quite similar, a decrease in full-width half-maximum (FWHM) was clearly noticed, indicating catalyst sintering. Compared to pre-exposure, post-exposure crystallite size was found to have increased from 11 to 13 nm, whereas particle size was doubled from 313 to 612 nm. However, the sign of sintering or deactivation was not clearly observed in TOS experiment. This could be due to the fact that the rate of reaction is rapid, to the point that the catalyst surface area becomes relatively less significant. No NiO peak was found on the diffraction pattern in either the pre- or post-exposure, indicating that the catalyst was fully reduced as peaks appeared at 44.508, 51.847, and 76.372 (JCPDS No. 00-004-0850). However, surface morphology of the pre- and post-exposure catalyst were found to be different, as shown in Figure 8. It can be seen that the particle size of the catalyst became larger after reaction due to its agglomeration, in an attempt to reduce its surface free energy.

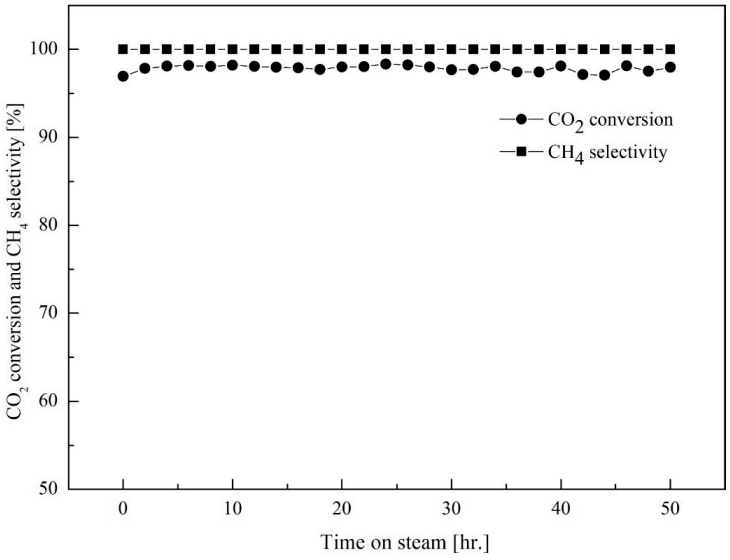

Figure 6. Time on steam of 40%wt. NiO/CeO_2-Cr_2O_3 after H_2/CO_2 = 4:1 exposure at 290 °C and 27,624 $mL.h^{-1}.g_{cat}{}^{-1}$ for 50 h.

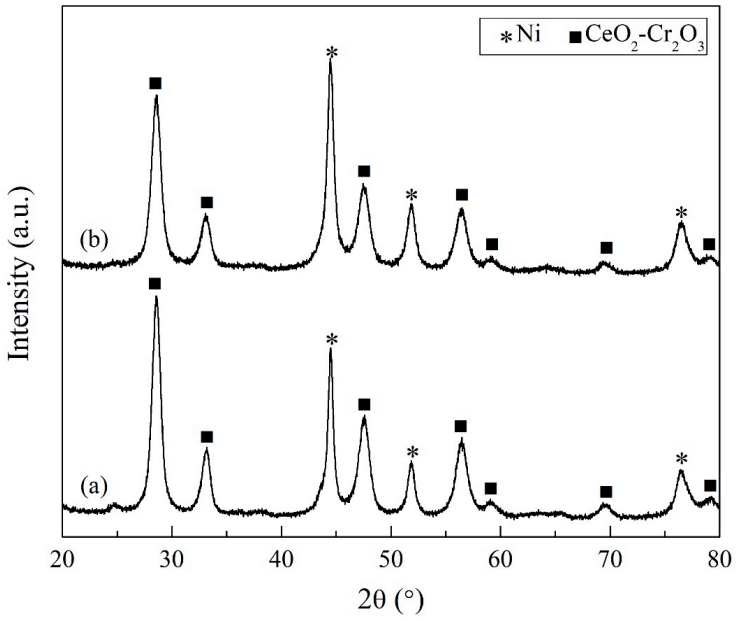

Figure 7. XRD patterns of 40%wt. NiO/CeO_2-Cr_2O_3: (**a**) before reaction and (**b**) after stability, where Ni (*) and CeO_2-Cr_2O_3 (■) phases.

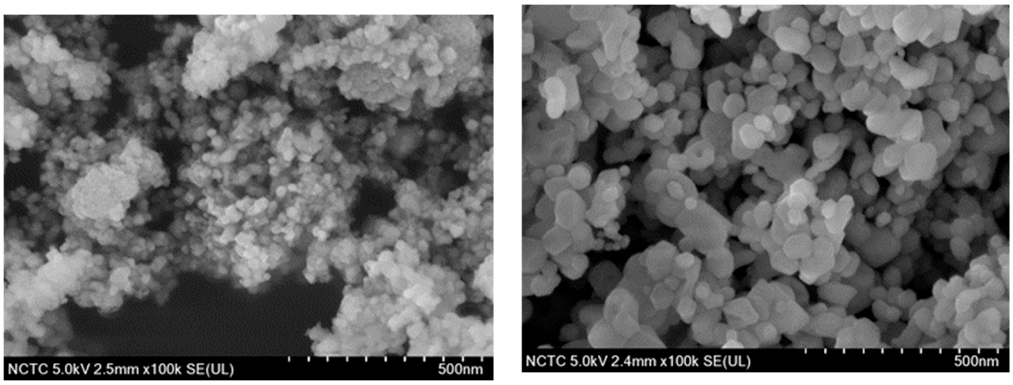

Figure 8. Surface morphology of 40%wt. NiO/CeO_2-Cr_2O_3 at magnitude × 100,000: before (**Left**) reaction and after (**Right**) stability.

The catalyst performance was compared between this work and other works that researched other catalysts (i.e., $10Ni/CeO_2$ [42], $10Ni/CeO_2$-ZrO_2 (CZ) [19], 15Ni/CZ, 15Ni-3Fe/CZ, 15Ni-3Co/CZ [42], 40Ni/CZ [3], $15Ni-2Ce/Al_2O_3$ [50], 5Ni/CZ [51], $20Ni/Al_2O_3$ [52], and $40Ni-5Ce/Al_2O_3$ [47]); as shown in Figure 9. Ni/CeO_2-Cr_2O_3 catalyst can be deemed as a superior catalyst due to its high catalytic activity (Y_{CH4} > 95% zone) at low operating temperatures.

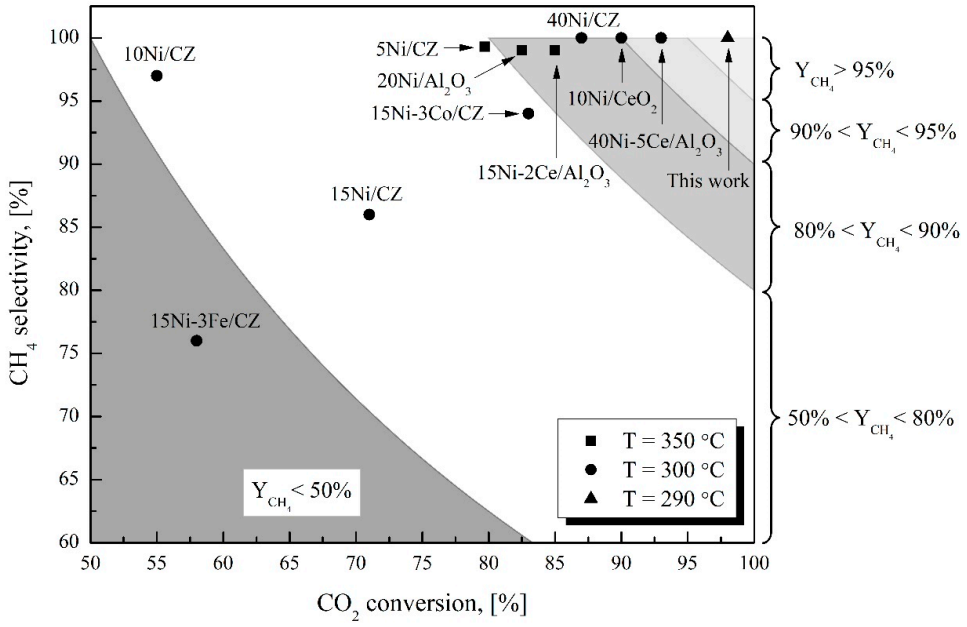

Figure 9. The summaries of the catalytic performances toward CO_2 methanation over various catalysts at H_2/CO_2 = 4:1.

4. Conclusions

The screening of monometallic catalysts (i.e., Ni, Fe and Co) doped on CeO_2-Cr_2O_3 support was studied in a milli-packed bed reactor. All the catalysts were prepared using one-pot hydrolysis. Ni was proven to be the most effective dopant. The amount of Ni loading was found optimal at 40% by weight, giving CO_2 conversion of 98.7% and CH_4 selectivity of 100% at a relatively low temperature of 290 °C. At temperatures of 200 to 350 °C, the reaction was kinetically driven by the higher operating temperature. However, thermodynamic limitation took place at temperatures higher than 350 °C where a drop in catalytic performance was observed. The catalyst was also stable during 50 h time on stream experiment. $Ni-CeO_2/Cr_2O_3$ was proven to be one of the highest potential catalysts for the CO_2 hydrogenation process of CH_4 production.

Author Contributions: Conceptualization, U.W.H. and V.T.; methodology, V.T.; software, C.K.; validation, S.A., M.H.; formal analysis, S.A.; investigation, C.K.; resources, N.L. and U.W.H.; data curation, N.L.; writing—original draft preparation, V.T. and C.K.; writing—review and editing, M.H.; visualization, N.L.; supervision, N.L. and U.W.H.; project administration, V.T.; funding acquisition, U.W.H. All authors have read and agreed to the published version of the manuscript.

Funding: This research was funded by National Research Council of Thailand (NRCT) contract number (1) N41A640149, (2) 668/2563 and (3) 130/2563; and King Mongkut's University of Technology North Bangkok contract number (1) KMUTNB-BasicR-64-34, (2) KMUTNB-BasicR-64-31, and (3) KMUTNB-PHD-62-10.

Conflicts of Interest: The authors declare no conflict of interest.

References

1. Blunden, J.; Arndt, D.S. State of the Climate in 2018. *Bull. Am. Meteorol. Soc.* **2019**, *100*, S1–S429. [CrossRef]
2. Cheah, W.Y.; Ling, T.C.; Juan, J.C.; Lee, D.-J.; Chang, J.-S.; Show, P.L. Biorefineries of carbon dioxide: From carbon capture and storage (CCS) to bioenergies production. *Bioresour. Technol.* **2016**, *215*, 346–356. [CrossRef]
3. Nie, W.; Zou, X.; Chen, C.; Wang, X.; Ding, W.; Lu, X. Methanation of Carbon Dioxide over Ni–Ce–Zr Oxides Prepared by One-Pot Hydrolysis of Metal Nitrates with Ammonium Carbonate. *Catalysts* **2017**, *7*, 104. [CrossRef]
4. Gao, J.; Liu, Q.; Gu, F.; Liu, B.; Zhong, Z.; Su, F. Recent advances in methanation catalysts for the production of synthetic natural gas. *RSC Adv.* **2015**, *5*, 22759–22776. [CrossRef]
5. Chisholm, G.; Cronin, L. *Hydrogen from Water Electrolysis*; Elsevier: Amsterdam, The Netherlands, 2016; pp. 315–343.
6. Huynh, H.L.; Yu, Z. CO_2 Methanation on Hydrotalcite-Derived Catalysts and Structured Reactors: A Review. *Energy Technol.* **2020**, *8*. [CrossRef]
7. Kierzkowska-Pawlak, H.; Tyczkowski, J.; Balcerzak, J.; Tracz, P. Advances in plasma produced CoO_x-based nanocatalysts for CO_2 methanation. *Catal. Today* **2019**, *337*, 162–170. [CrossRef]
8. Zhao, B.; Chen, Z.; Chen, Y.; Ma, X. Syngas methanation over Ni/SiO_2 catalyst prepared by ammonia-assisted impregnation. *Int. J. Hydrog. Energy* **2017**, *42*, 27073–27083. [CrossRef]
9. Rostrup-Nielsen, J.; Pedersen, K.; Sehested, J. High temperature methanation: Sintering and structure sensitivity. *Appl. Catal. A Gen.* **2007**, *330*, 134–138. [CrossRef]
10. Moghaddam, S.V.; Rezaei, M.; Meshkani, F.; Daroughegi, R. Carbon dioxide methanation over Ni-M/Al_2O_3 (M: Fe, CO, Zr, La and Cu) catalysts synthesized using the one-pot sol-gel synthesis method. *Int. J. Hydrog. Energy* **2018**, *43*, 16522–16533. [CrossRef]
11. Shen, W.-J.; Okumura, M.; Matsumura, Y.; Haruta, M. The influence of the support on the activity and selectivity of Pd in CO hydrogenation. *Appl. Catal. A Gen.* **2001**, *213*, 225–232. [CrossRef]
12. Takoudis, C.G. The catalytic synthesis of hydrocarbons from H_2/CO mixtures over the group VIII metals: Comments on methanation kinetics. *J. Catal.* **1982**, *78*, 265. [CrossRef]
13. Tsiotsias, A.I.; Charisiou, N.D.; Yentekakis, I.V.; Goula, M.A. The Role of Alkali and Alkaline Earth Metals in the CO_2 Methanation Reaction and the Combined Capture and Methanation of CO_2. *Catalysts* **2020**, *10*, 812. [CrossRef]
14. Wang, F.; He, S.; Chen, H.; Wang, B.; Zheng, L.; Wei, M.; Evans, D.G.; Duan, X. Active Site Dependent Reaction Mechanism over Ru/CeO_2 Catalyst toward CO_2 Methanation. *J. Am. Chem. Soc.* **2016**, *138*, 6298–6305. [CrossRef] [PubMed]
15. Le, T.A.; Kim, M.S.; Lee, S.H.; Kim, T.W.; Park, E.D. CO and CO_2 methanation over supported Ni catalysts. *Catal. Today* **2017**, *293-294*, 89–96. [CrossRef]
16. Liu, Q.; Zhong, Z.; Gu, F.; Wang, X.; Lu, X.; Li, H.; Xu, G.; Su, F. CO methanation on ordered mesoporous Ni–Cr–Al catalysts: Effects of the catalyst structure and Cr promoter on the catalytic properties. *J. Catal.* **2016**, *337*, 221–232. [CrossRef]
17. Dufour, J.; Martos, C.; Ruiz, A.; Ayuela, F. Effect of the precursor on the activity of high temperature water gas shift catalysts. *Int. J. Hydrog. Energy* **2013**, *38*, 7647–7653. [CrossRef]
18. Lohitharn, N.; Goodwinjr, J. Impact of Cr, Mn and Zr addition on Fe Fischer–Tropsch synthesis catalysis: Investigation at the active site level using SSITKA. *J. Catal.* **2008**, *257*, 142–151. [CrossRef]
19. Ashok, J.; Ang, M.; Kawi, S. Enhanced activity of CO_2 methanation over Ni/CeO_2-ZrO_2 catalysts: Influence of preparation methods. *Catal. Today* **2017**, *281*, 304–311. [CrossRef]
20. Wang, X.; Zhu, L.; Liu, Y.; Wang, S. CO_2 methanation on the catalyst of Ni/MCM-41 promoted with CeO_2. *Sci. Total Environ.* **2018**, *625*, 686–695. [CrossRef] [PubMed]
21. Branco, J.; Silva, R.; Ferreira, A. Methanation of CO_2 over Cobalt-Lanthanide Aerogels: Effect of Calcination Temperature. *Catalysts* **2020**, *10*, 704. [CrossRef]
22. Wang, H.; Tsilomelekis, G. Catalytic performance and stability of Fe-doped CeO_2 in propane oxidative dehydrogenation using carbon dioxide as an oxidant. *Catal. Sci. Technol.* **2020**, *10*, 4362–4372. [CrossRef]
23. Konishcheva, M.; Potemkin, D.; Snytnikov, P.; Zyryanova, M.; Pakharukova, V.; Simonov, P.; Sobyanin, V. Selective CO methanation in H_2-rich stream over Ni–, Co– and Fe/CeO_2: Effect of metal and precursor nature. *Int. J. Hydrog. Energy* **2015**, *40*, 14058–14063. [CrossRef]

24. Jalama, K. Carbon dioxide hydrogenation over nickel-, ruthenium-, and copper-based catalysts: Review of kinetics and mechanism. *Catal. Rev.* **2017**, *59*, 95–164. [CrossRef]
25. Aziz, M.; Jalil, A.; Triwahyono, S.; Saad, M. CO_2 methanation over Ni-promoted mesostructured silica nanoparticles: Influence of Ni loading and water vapor on activity and response surface methodology studies. *Chem. Eng. J.* **2015**, *260*, 757–764. [CrossRef]
26. Singh, P.; Hegde, M.S. $Ce_{0.67}Cr_{0.33}O_{2.11}$: A New Low-Temperature O_2 Evolution Material and H_2 Generation Catalyst by Thermochemical Splitting of Water. *Chem. Mater.* **2010**, *22*, 762–768. [CrossRef]
27. Hu, Q.; Yue, B.; Shao, H.; Yang, F.; Wang, J.; Wang, Y.; Liu, J. Facile syntheses of cerium-based $CeMO_3$ (M = Co, Ni, Cu) perovskite nanomaterials for high-performance supercapacitor electrodes. *J. Mater. Sci.* **2020**, *55*, 8421–8434. [CrossRef]
28. Shannon, R.D. Revised effective ionic radii and systematic studies of interatomic distances in halides and chalcogenides. *Acta Crystallogr. A* **1976**, *32*, 751–767. [CrossRef]
29. Ghiasi, M.; Malekzadeh, A. Structural Features of (Ce, La or Sr)(Mn or Co)O_3 Nano-Perovskites as a Catalyst for Carbon Monoxide Oxidation. *Acta Met. Sin.* **2014**, *27*, 635–641. [CrossRef]
30. Qiu, Y.; Ye, N.; Situ, D.; Zuo, S.; Wang, X. Study of Catalytic Combustion of Chlorobenzene and Temperature Programmed Reactions over CrCeOx/AlFe Pillared Clay Catalysts. *Materials* **2019**, *12*, 728. [CrossRef]
31. Li, W.; Liu, H.; Chen, Y. Promotion of transition metal oxides on the NH_3-SCR performance of ZrO_2-CeO_2 catalyst. *Front. Environ. Sci. Eng.* **2017**, *11*, 6. [CrossRef]
32. Yang, P.; Yang, S.; Shi, Z.; Meng, Z.; Zhou, R. Deep oxidation of chlorinated VOCs over CeO_2 -based transition metal mixed oxide catalysts. *Appl. Catal. B Environ.* **2015**, *162*, 227–235. [CrossRef]
33. Liu, H.; Wei, L.; Yue, R.; Chen, Y. CrOx–CeO_2 binary oxide as a superior catalyst for NO reduction with NH_3 at low temperature in presence of CO. *Catal. Commun.* **2010**, *11*, 829–833. [CrossRef]
34. Xu, X.; Li, L.; Yu, F.; Peng, H.; Fang, X.; Wang, X. Mesoporous high surface area NiO synthesized with soft templates: Remarkable for catalytic CH_4 deep oxidation. *Mol. Catal.* **2017**, *441*, 81–91. [CrossRef]
35. Khajonvittayakul, C.; Tongnan, V.; Kangsadan, T.; Laosiripojana, N.; Jindasuwan, S.; Hartley, U.W. Thermodynamic and mechanism study of syngas production via integration of nitrous oxide decomposition and methane partial oxidation in the presence of 10%NiO–$La_{0.3}Sr_{0.7}Co_{0.7}Fe_{0.3}O_{3-\delta}$. *React. Kinet. Mech. Catal.* **2019**, *127*, 839–855. [CrossRef]
36. Khajonvittayakul, C.; Tongnan, V.; Namo, N.; Phonbubpha, C.; Laosiripojana, N.; Hartley, M.; Hartley, U.W. Tar steam reforming for synthesis gas production over Ni-based on ceria/zirconia and $La_{0.3}Sr_{0.7}Co_{0.7}Fe_{0.3}O_3$ in a packed-bed reactor. *Chemosphere* **2021**, *277*. [CrossRef]
37. Saharuddin, T.S.T.; Samsuri, A.; Salleh, F.; Othaman, R.; Bin Kassim, M.; Hisham, M.W.M.; Yarmo, M.A. Studies on reduction of chromium doped iron oxide catalyst using hydrogen and various concentration of carbon monoxide. *Int. J. Hydrog. Energy* **2017**, *42*, 9077–9086. [CrossRef]
38. Reddy, G.K.; Gunasekara, K.; Boolchand, P.; Smirniotis, P.G. Cr- and Ce-Doped Ferrite Catalysts for the High Temperature Water−Gas Shift Reaction: TPR and Mossbauer Spectroscopic Study. *J. Phys. Chem. C* **2010**, *115*, 920–930. [CrossRef]
39. Díaz, E.; Ordóñez, S.; Vega, A.; Coca, J. Catalytic combustion of hexane over transition metal modified zeolites NaX and CaA. *Appl. Catal. B Environ.* **2005**, *56*, 313–322. [CrossRef]
40. Stangeland, K.; Kalai, D.; Li, H.; Yu, Z. CO_2 Methanation: The Effect of Catalysts and Reaction Conditions. *Energy Procedia* **2017**, *105*, 2022–2027. [CrossRef]
41. Tada, S.; Shimizu, T.; Kameyama, H.; Haneda, T.; Kikuchi, R. Ni/CeO_2 catalysts with high CO_2 methanation activity and high CH_4 selectivity at low temperatures. *Int. J. Hydrog. Energy* **2012**, *37*, 5527–5531. [CrossRef]
42. Pastor-Pérez, L.; Saché, E.; Jones, C.; Gu, S.; Arellano-Garcia, H.; Reina, T. Synthetic natural gas production from CO_2 over Ni-x/CeO_2-ZrO_2 (x = Fe, Co) catalysts: Influence of promoters and space velocity. *Catal. Today* **2018**, *317*, 108–113. [CrossRef]
43. Aziz, M.; Jalil, A.; Triwahyono, S.; Mukti, R.; Taufiq-Yap, Y.; Sazegar, M. Highly active Ni-promoted mesostructured silica nanoparticles for CO_2 methanation. *Appl. Catal. B Environ.* **2014**, *147*, 359–368. [CrossRef]
44. Lu, B.; Kawamoto, K. Preparation of the highly loaded and well-dispersed NiO/SBA-15 for methanation of producer gas. *Fuel* **2013**, *103*, 699–704. [CrossRef]
45. Yamasaki, M.; Habazaki, H.; Asami, K.; Izumiya, K.; Hashimoto, K. Effect of tetragonal ZrO_2 on the catalytic activity of Ni/ZrO_2 catalyst prepared from amorphous Ni–Zr alloys. *Catal. Commun.* **2006**, *7*, 24–28. [CrossRef]
46. Perkas, N.; Amirian, G.; Zhong, Z.; Teo, J.; Gofer, Y.; Gedanken, A. Methanation of Carbon Dioxide on Ni Catalysts on Mesoporous ZrO_2 Doped with Rare Earth Oxides. *Catal. Lett.* **2009**, *130*, 455–462. [CrossRef]
47. Gac, W.; Zawadzki, W.; Rotko, M.; Słowik, G.; Greluk, M. CO_2 Methanation in the Presence of Ce-Promoted Alumina Supported Nickel Catalysts: H_2S Deactivation Studies. *Top. Catal.* **2019**, *62*, 524–534. [CrossRef]
48. Wongsartsai, C.; Tongnan, V.; Sornchamni, T.; Siri-Nguan, N.; Laosiripojana, N.; Hartley, M.; Hartley, U.W. CO_2 utilization via methanation using 40%Ni/$CexCr_1$-xO_2 as a novel catalyst: A comparative study of packed-bed and micro-channel reactors. *React. Kinet. Mech. Catal.* **2020**, *131*, 1–17. [CrossRef]
49. Bacariza, C.; Graça, I.; Westermann, A.; Ribeiro, M.F.; Lopes, J.; Henriques, C. CO_2 Hydrogenation Over Ni-Based Zeolites: Effect of Catalysts Preparation and Pre-reduction Conditions on Methanation Performance. *Top. Catal.* **2015**, *59*, 314–325. [CrossRef]
50. Liu, H.; Zou, X.; Wang, X.; Lu, X.; Ding, W. Effect of CeO_2 addition on Ni/Al_2O_3 catalysts for methanation of carbon dioxide with hydrogen. *J. Nat. Gas Chem.* **2012**, *21*, 703–707. [CrossRef]

51. Ocampo, F.; Louis, B.; Kiennemann, A.; Roger, A.-C. CO2 methanation over Ni-Ceria-Zirconia catalysts: Effect of preparation and operating conditions. In *IOP Conference Series: Materials Science and Engineering*; IOP Publishing: Bristol, UK, 2011; Volume 19, p. 012007. [CrossRef]
52. Sepehri, S.; Rezaei, M. Preparation of Highly Active Nickel Catalysts Supported on Mesoporous Nanocrystallineγ-$Al_2O_3$for Methane Autothermal Reforming. *Chem. Eng. Technol.* **2015**, *38*, 1637–1645. [CrossRef]